X-shaped Radical Offshore Wind Turbine for Overall Cost of Energy Reduction

D2.6

Results of multibody analysis (of X-ROTOR concept)

https://xrotor-project.eu

@XROTORProject

September 2022

This project has received funding from the European Union's Horizon 2020 research and innovation programme under grant agreement No 101007135

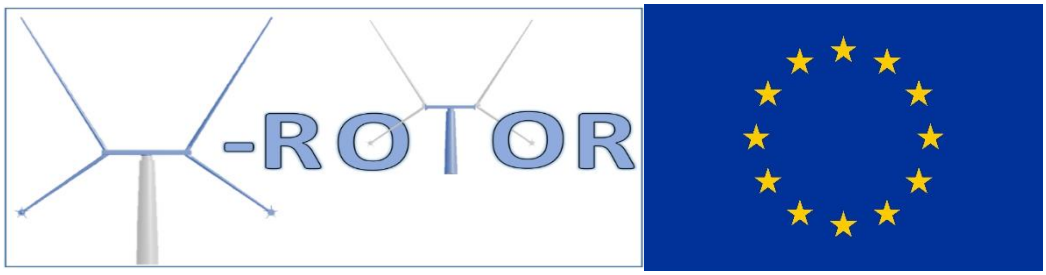

X-SHAPED RADICAL OFFSHORE WIND TURBINE FOR OVERALL COST OF ENERGY REDUCTION

Project acronym: **XROTOR**
Grant agreement number: 101007135
Start date: 01st January 2021
Duration: 3 years

WP2 Aero-elastic code development and performance
T2.6 – Validation of the X-Rotor concept using Multibody Analysis
D2.6 Report and date related to the multibody analysis of the XROTOR concept-

Lead Beneficiary: CENER
Delivery date: 20th September 2022

Author(s) information (alphabetical):		
Name	**Organisation**	**Email**
Roberto Montejo	CENER	rmontejo@cener.com
Aurelio Cascales	CENER	acascales@cener.com
Beatriz Méndez	CENER	bmendez@cener.com

Document Information

Version	Date	Description	Prepared by	Reviewed by	Approved by
1	20.09.2022	V1.0	CENER	W. Leithead & J. Carroll	Professor W. Leithead

The XROTOR Project has received funding from the European Union's Horizon 2020 research and innovation programme under grant agreement no. 101007135.

Executive Summary

Deliverable Description:

This deliverable report supports deliverable D2.6 *"Validation of the X-ROTOR concept using Multibody Analysis"* and details the results of the study performed over the X-Rotor primary rotor. Wind turbine loads have been obtained from the Aeroelastic Dynamic model output from Task 2.1 and the load cases evaluated in Task 2.4.

Responsible:

The responsible partner is the CENER, with Roberto Montejo as the principle investigator.

Outcome Summary:

This deliverable contains the X-ROTOR primary rotor multibody analysis, as well as the conclusions to improve the blade definition to advance with the concept to higher TRL levels.

Content

List of Figures 3
List of Tables 4
Deliverable details 5
Assumptions for the multibody analysis 6
Blade´s finite element model 7
Primary rotor multibody model 9
a) Bodies 9
b) Joints 13
c) Loads 13
Load cases description 16
Conclusions 18
Disclaimer 21
Copyright Notice 21

List of Figures

Figure 1 Multibody model general configuration 6
Figure 2 Azimuth position and pitch angle convection 7
Figure 3 Provided blades' internal configuration preliminary design and material properties 7
Figure 4 FE model. Different properties along upper blade and 2D CQUAD elements size detail 8
Figure 5 FE model. Rigid RBE2's location at 18 sections along upper blade spanwise 8
Figure 6 Visual representation of thickness of CQUAD properties at root section. Added core at shell areas can be noted 9
Figure 7 Upper and lower blades finite element models 9
Figure 8 Tower and cross arm rigid body (red) and its center of mass local coordinate 10
Figure 9 Local coordinate system at blade root's pitch point 11
Figure 10 Upper Blade's (cyan colour) pitch position depending on wind speed (top view) 12
Figure 11 Roots' attachment location 12
Figure 12 Alternative roots' attachment location ahead 12
Figure 13 Effective joints in the model 13
Figure 14 Load graphs (normal and tangential forces, and pitch moment) for one particular point in blade 14
Figure 15 Direction of aerodynamic loads on blades. X-Rotor position on 90°/270° azimuth plane 15
Figure 16 All points' load graphics (force and moment) at a particular time instant 15
Figure 17 Torque applied (kNm) by imposed motion along 30s 16
Figure 18 Torque applied (red curve, kNm) by imposed motion up to 32s, and subsequent constant applied resistant torque (blue curve, kNm) when imposed motion is turn off 17
Figure 19 Torques applied (red and blue curves, kNm) along the analysis and tower angular velocity (green curve, deg/s) 17
Figure 20 Torque (kNm) at tower with rigid and flexible blades, and azimuth position (deg) 18
Figure 21 Structure configuration including secondary rotors at lower blades' tips 19
Figure 22 Load graphics with secondary rotors configuration (thrust forces in blue) 20

List of Tables

Table 1 Tower and cross arm mass properties.....10
Table 2 Blades' mass properties at root's local coordinate 11

Deliverable details

This deliverable is organized as follows: first the blade structural definition used to perform the multibody analysis is described, then the assumptions made to perform the analyses are summarized as well as the load cases evaluated. Finally, the results and conclusions will summarize the key outcomes of this study.

Assumptions for the multibody analysis

Primary rotor tower and its cross arm are defined as rigid bodies. Blades are included as flexible bodies, although comparative analyses when considering these blades as rigid parts are performed later. In this model, secondary rotors are only considered as dead weights (10t each) attached near of lower blades' tips, and a virtual generator at the tower of the primary rotor is supposed to apply the resistant torque.

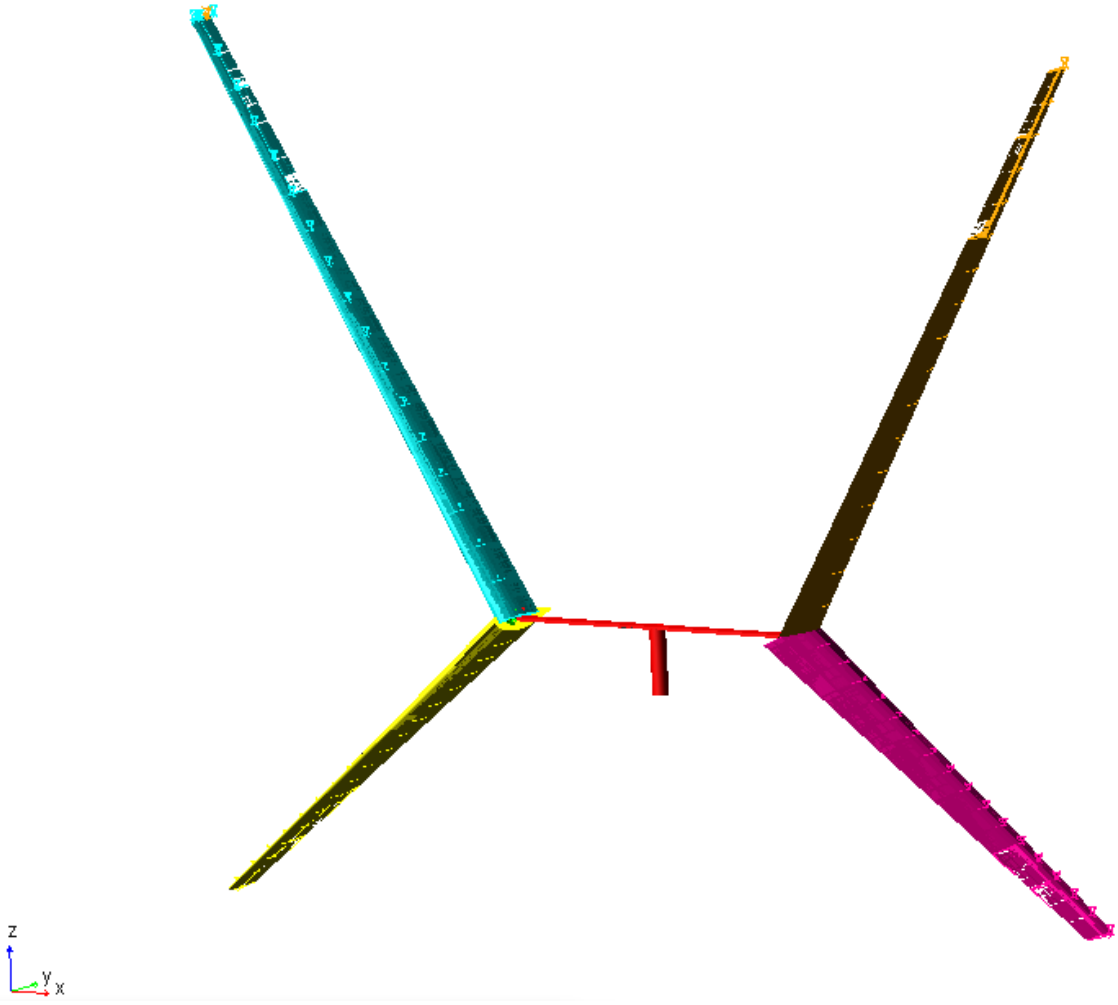

Figure 1 Multibody model general configuration

Next picture shows the selected convection for angles and directions in the model.

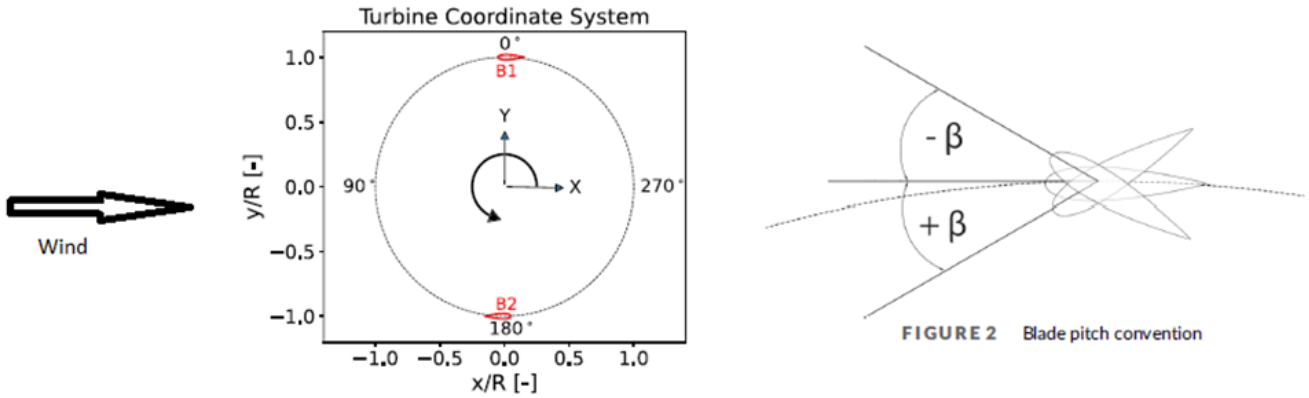

FIGURE 1 Turbine coordinate system, wind approaches from 90°

FIGURE 2 Blade pitch convention

Figure 2 Azimuth position and pitch angle convection

Multibody analysis software MSC.ADAMS' methodology for introduction of flexible bodies is based on the Craig-Bampton approach to component mode synthesis (CMS). Modal definition of these flexible bodies is firstly calculated through a finite element analysis (FEA) for each part.

Blade´s finite element model

Blades' FE models were defined from geometrical data and material properties provided. These models are made up with 2D quadrilateral elements of 4 nodes (Nastran CQUAD4) on which laminate plies are defined (PCOMP properties card), and rigid MPC (RBE2) for aerodynamic loads' introduction points (67 for each lower blade and 72 for each upper blade) at 18 sections along blade spanwise. These MPC's are defined on the spar cap, except for the root section where whole profile is rigidized and it will be used for attachment to cross arm.

3.3.1. Primary rotor blade design

The primary rotor blades consist of symmetric aerofoil profiles, which are strengthened by two spar caps that take most of the bending loads. The spar caps are connected by two parallel shear webs. The blade shell is also reinforced at the leading and trailing edges. In Figure 14 the layout of blade internals at an arbitrary cross section is indicated.

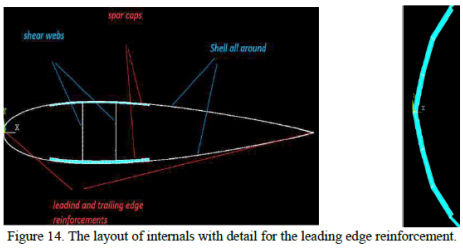

Figure 14. The layout of internals with detail for the leading edge reinforcement.

Table 3. Mechanical properties of blade components

	Shell	Spar cap	Reinforcement	Shear webs
Property	Triaxial	Uniaxial (CF)	Uniaxial (GF)	Biaxial
E11 [GPa]	21.790	115.00	41.630	13.920
E22 [GPa]	14.670	7.560	14.930	13.920
v12 [-]	0.478	0.30	0.241	0.533
G12 [GPa]	9.413	3.96	5.047	11.500
p [Kg/m3]	1845.000	1578	1915.000	1845.000
σ11-Ten [MPa]	480.400	1317.60	876.100	223.200
σ11-Comp [MPa]	393.000	620.13	625.800	209.200
σ22-Ten [MPa]	90.400	21.88	74.030	223.200
σ 22-Comp [MPa]	152.700	76.25	189.400	209.200
τ 12 [MPa]	114.000	45.53	56.580	140.300

Figure 3 Provided blades' internal configuration preliminary design and material properties

Next picture shows the different properties defined on blade elements as a color code, and a detail of the CQUAD4 elements on the model.

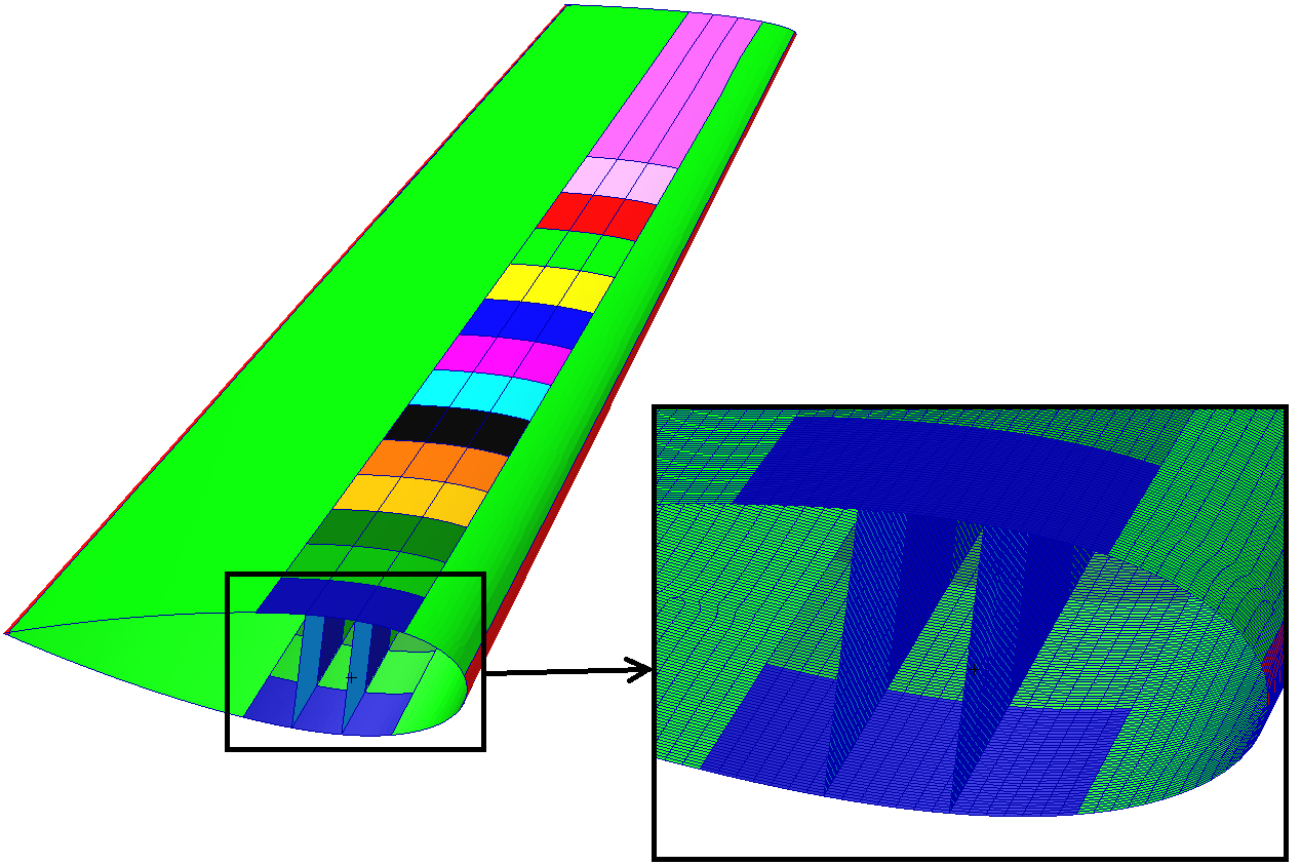

Figure 4 FE model. Different properties along upper blade and 2D CQUAD elements size detail

The MPC distribution along blade for load input is shown in the next figure

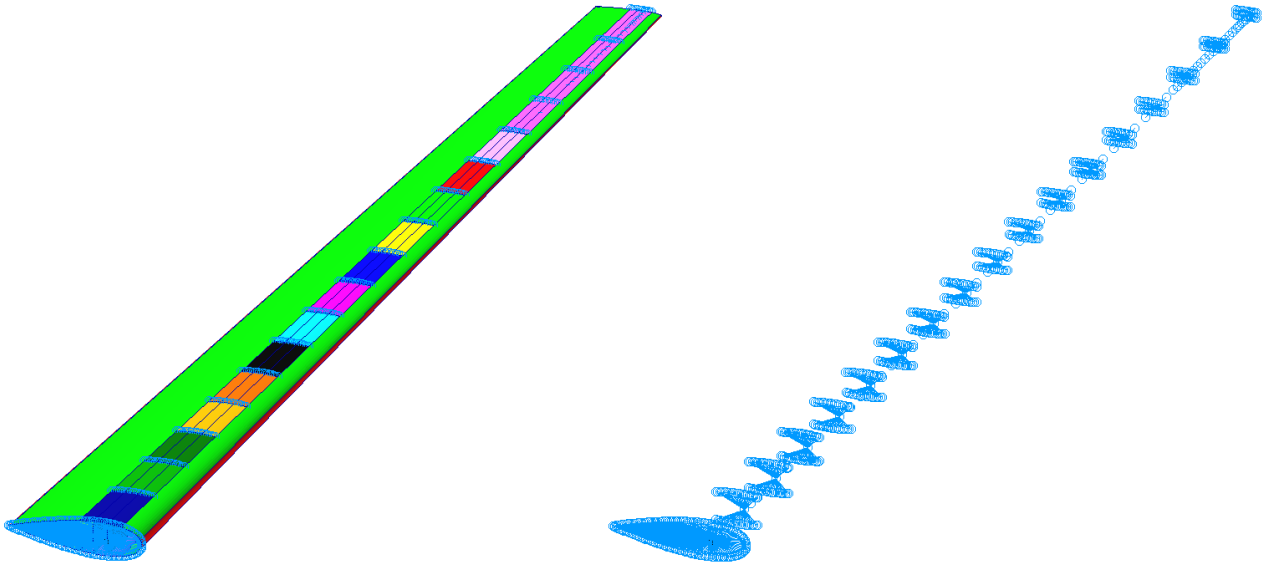

Figure 5 FE model. Rigid RBE2's location at 18 sections along upper blade spanwise

Given that blades are at initial design, some parameters which do not affect main properties (stiffness and mass), are not defined yet. For example, there is no core defined for the shell. This results in a bunch of local modes when running a modal analysis as the like needed for flex body definition. For this reason, some arbitrary core thickness was included to supply local inertia at blade shells.

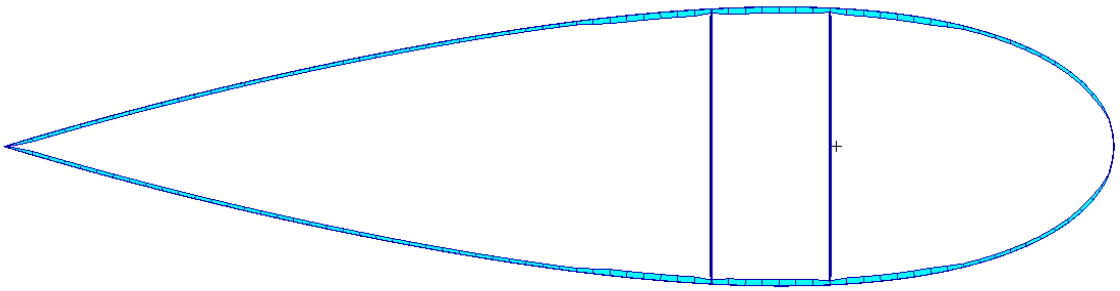

Figure 6 Visual representation of thickness of CQUAD properties at root section. Added core at shell areas can be noted

Next picture shows both upper and lower blade FE models

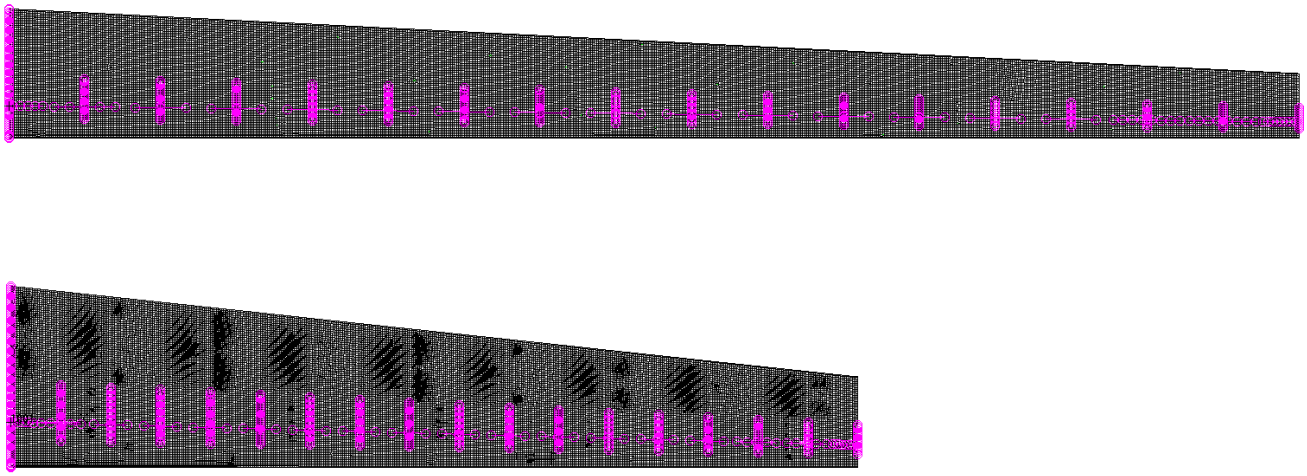

Figure 7 Upper and lower blades finite element models

Primary rotor multibody model

As stated before, this multibody simulation (MBS) only comprises the primary rotor of the X-ROTOR configuration, and resistant torque was applied at a virtual generator located at tower axis. This is not the case for real X-ROTOR structure, but lack of definition of secondary rotors at the moment does not allow to define a more accurate representation. In any case, a model with more appropriate reaction forces' location at secondary rotors is sketched later.

a) Bodies

The principal structure, vertical tower and cross arm, is considered as a unique rigid body. With this assumption and taking into account that most of the rotational inertia of the structure will be provided by blades (and secondary rotors), it is quite not indispensable the real geometry of these parts. For the analysis, the part is assumed to be steel. Next table shows resulting mass properties of the body; they might be not realistic, but as stated before, they will not have critical influence on the overall current analysis.

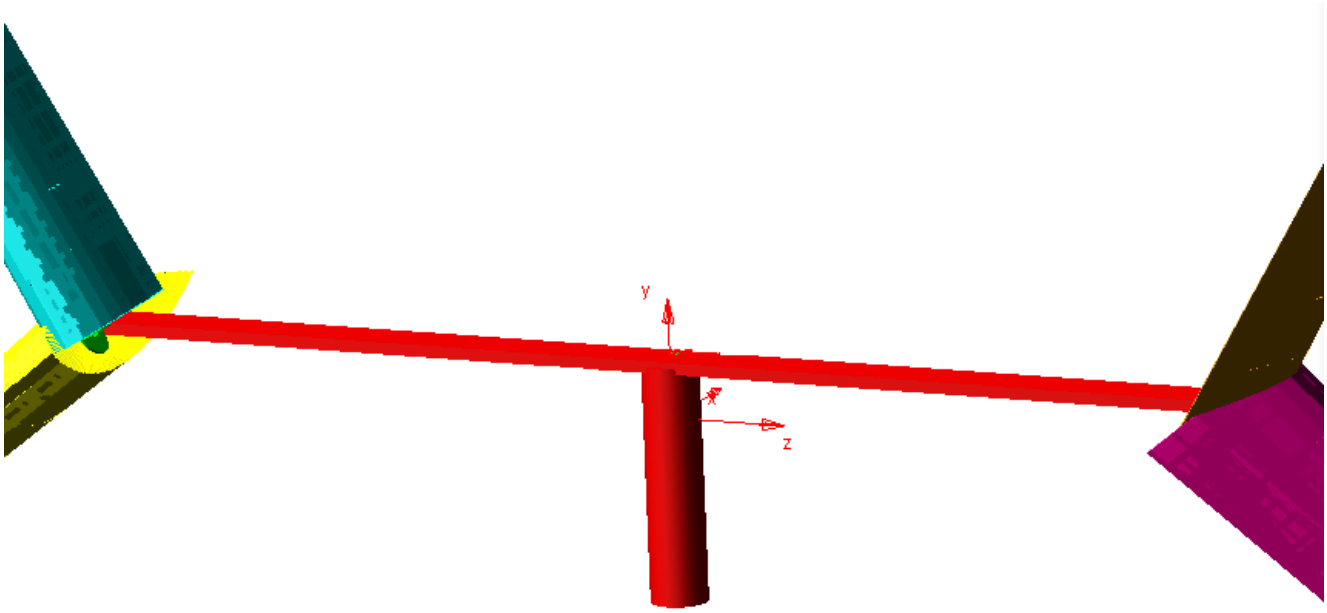

Figure 8 Tower and cross arm rigid body (red) and its center of mass local coordinate

Table 1 Tower and cross arm mass properties

Tower and Cross Arm		
Mass:	755000	kg
Inertia Tensor at cog local coordinate:		
I_{XX}	96.8E+06	kg m^2
I_{YY}	89.4E+06	kg m^2
I_{ZZ}	7.9E+06	kg m^2
I_{XY}	0.0E+00	kg m^2
I_{ZX}	0.0E+00	kg m^2
I_{YZ}	0.0E+00	kg m^2

Blades are included as flexible bodies and their modal definition have been detailed before. There are some intermediate rigid bodies defined between main cross arm and blades modeling the pitch system but they are not relevant for the current analysis where they remain fixed.

Table 2 summarizes resultant mass properties of each of the blades respect its local coordinate system, located at 25% of chord at root and oriented as shown in the next figure.

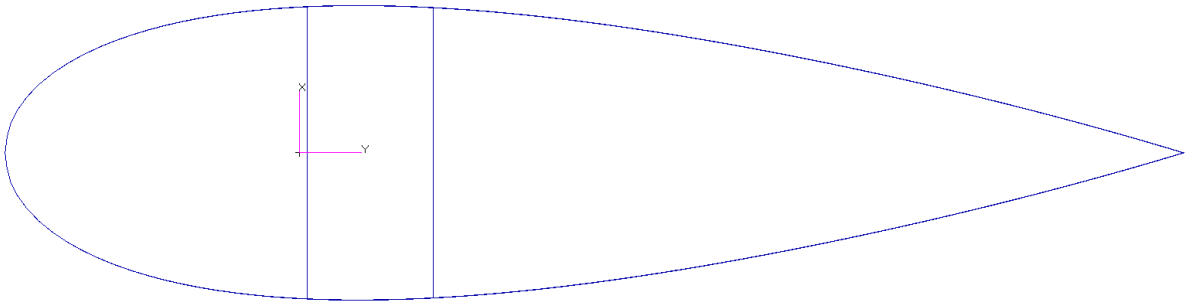

Figure 9 Local coordinate system at blade root's pitch point

Table 2 Blades' mass properties at root's local coordinate

UPPER BLADE			LOWER BLADE		
Mass:	40500	kg	Mass:	23384	kg
CM location:			CM location:		
X	0	m	X	0	m
Y	0.7	m	Y	1.4	m
Z	36.4	m	Z	27.0	m
Inertia Tensor:			Inertia Tensor:		
I_{XX}	81.5E+06	kg m^2	I_{XX}	25.1E+06	kg m^2
I_{YY}	81.4E+06	kg m^2	I_{YY}	24.8E+06	kg m^2
I_{ZZ}	0.2E+06	kg m^2	I_{ZZ}	0.3E+06	kg m^2
I_{XY}	0.0E+00	kg m^2	I_{XY}	0.0E+00	kg m^2
I_{ZX}	0.0E+00	kg m^2	I_{ZX}	0.0E+00	kg m^2
I_{YZ}	0.7E+06	kg m^2	I_{YZ}	0.6E+06	kg m^2

Blades, the only bodies to be considered as flexible, will have the root rigidly attached at edge points of the cross arm. Upper blades can be rotated around their pitch axes to proper orientation depending of wind speed. The pitch axis is located at 25% of chord length, and these axes for all blades are on a vertical plane containing the main vertical axis of rotation. This plane defines the azimuth position of the X-Rotor.

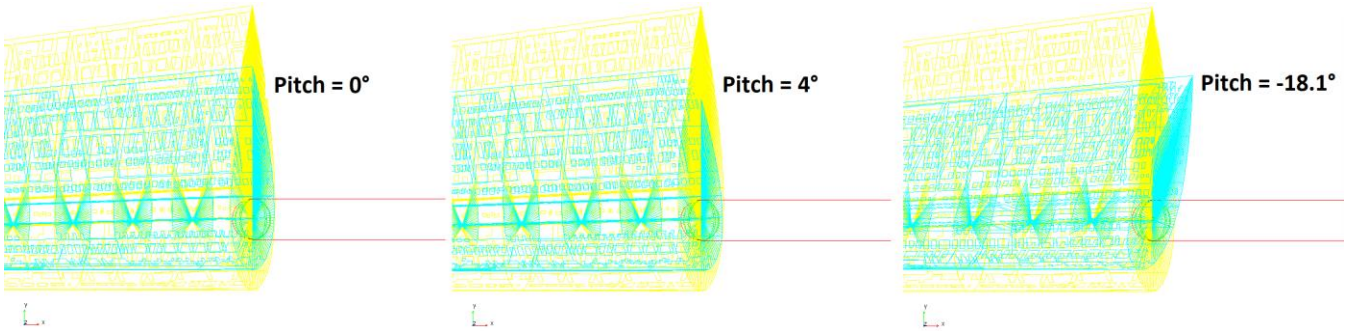

Figure 10 Upper Blade's (cyan colour) pitch position depending on wind speed (top view)

Blades are fixed to cross arm's symmetry plane at previous defined root local coordinate origin

ccccccccc

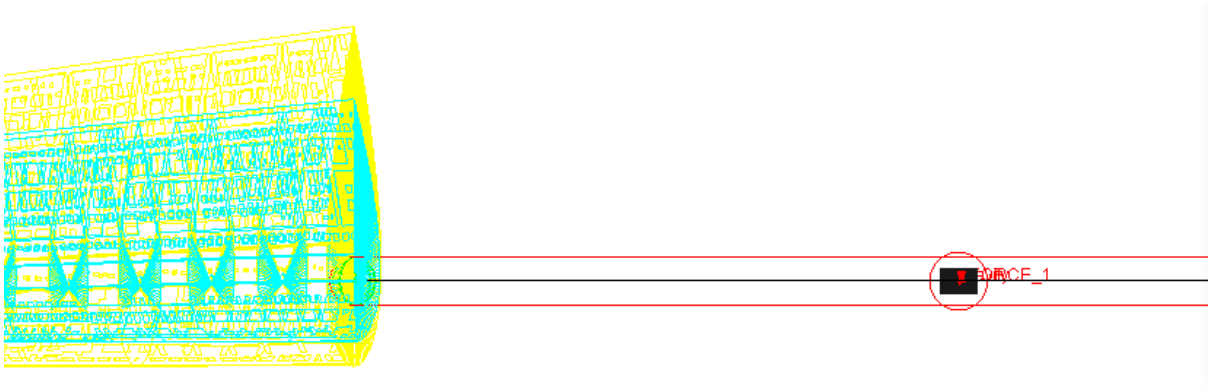

Figure 11 Roots' attachment location

It must be noted that slightly different position of the root blades, e.g. ahead of the azimuth plane, have great impact in the resultant torque on the structure due to application of predefined aerodynamic forces, so it must be guaranteed the concordance of these predefined aerodynamic forces generation and the position of the blades and azimuth plane on the model.

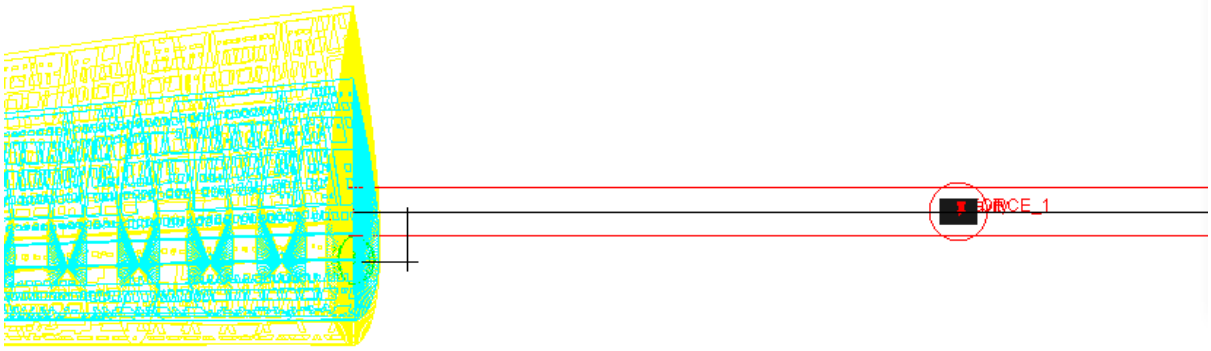

Figure 12 Alternative roots' attachment location ahead

A relevant characteristic in a dynamic simulation is the damping considered in the flexible bodies. It must be noted that the way aerodynamic forces are defined in the analysis limits the contribution of

aerodynamic damping, so the only damping input is the structural modal damping defined in the blades. This factor comprises different damping mechanisms which might be present in the model and it is usually tuned for each particular system attending to physical response.

b) Joints

Next image shows all the joints between bodies in the structure. Although upper blades can rotate and change the pitch, current simulation under constant wind speed keeps initial pitch position along time, so it becomes a rigid joint in fact. The only cinematic degree of freedom (excluding flexible blades themselves) is the rotation about the tower's vertical axis. This degree of freedom is cancelled when forced rotation is imposed, resulting in a zero cinematic degree of freedom model (excluding blade deformation).

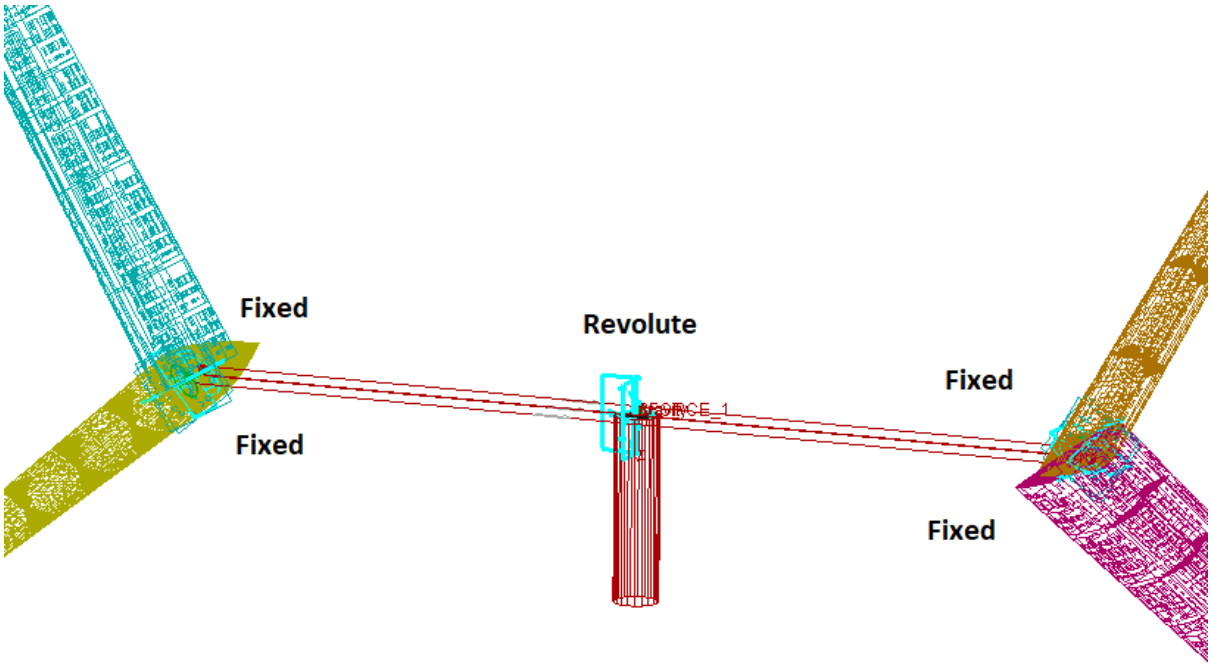

Figure 13 Effective joints in the model

c) Loads

Besides gravity, aerodynamic loads acting along blades are defined, dependent on the X-Rotor azimuth position and wind speed. Angular velocity is adjusted according to wind speed as well.

A resistant torque will be applied at the revolute joint location on tower. As it will be show later, two different ways to apply this torque are presented: as the necessary torque that rises up when a constant rotational motion is imposed in order to counteract the aerodynamic load on blades, or as an estimated constant resistant torque that maintains the structure rotating stationary.

For each force application point, several tables *load per length-azimuth position* have been provided for several *wind speed*. After computing the effective length that any of the load application points cover, this info results in a load response surface in a 3 axis graphics: *azimuth-wind speed-load*. Load has been separated in three components, *normal force, tangential force* and *pitch moment*, so three surface graphs are defined for each force application point (72 points for Upper Blades and 67 points for Lower Blades). This sums up a total of (72+67)x3 = 417 surface graphs. Next figure shows the three surfaces defining total load components for one of the points on lower blade.

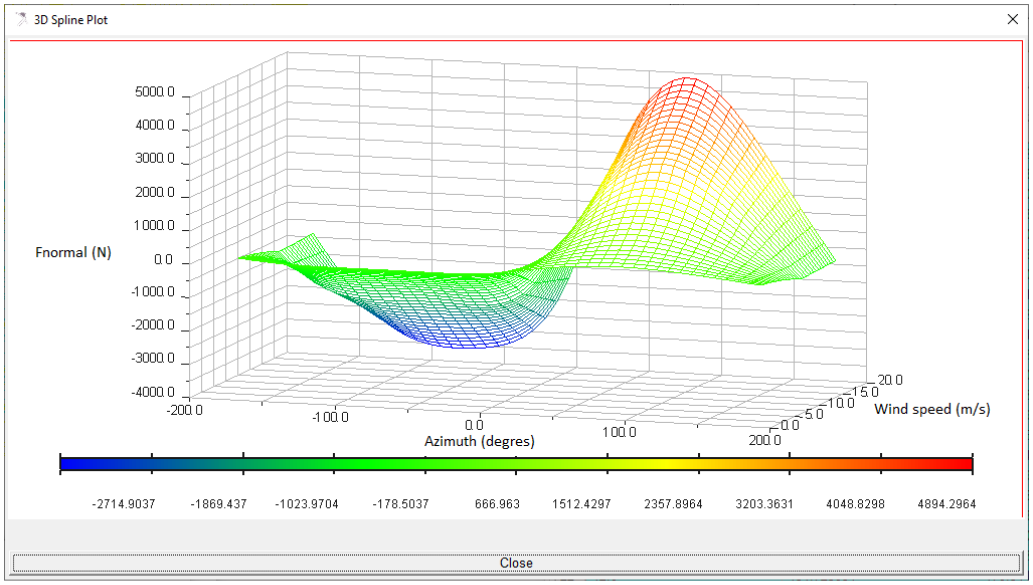

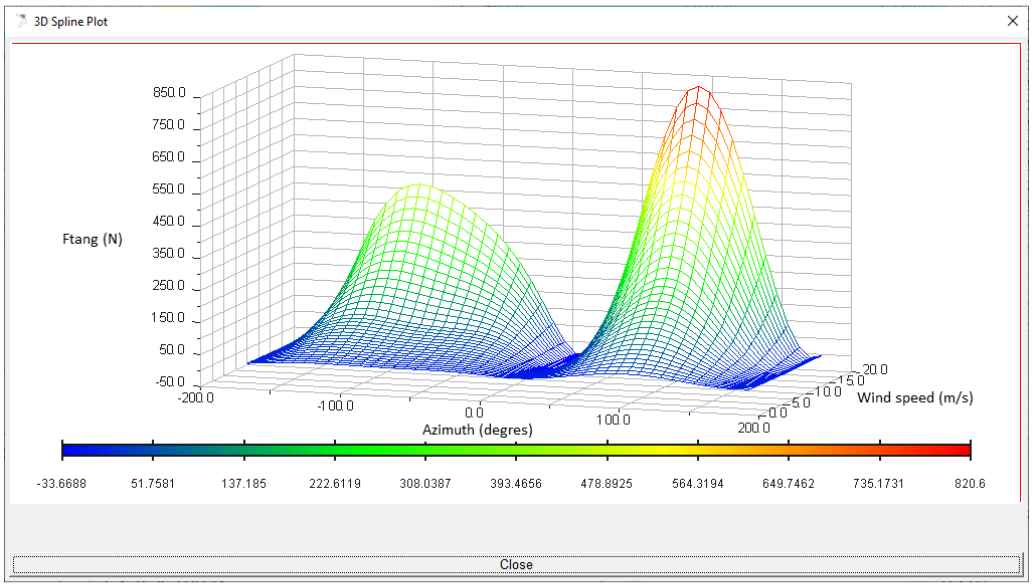

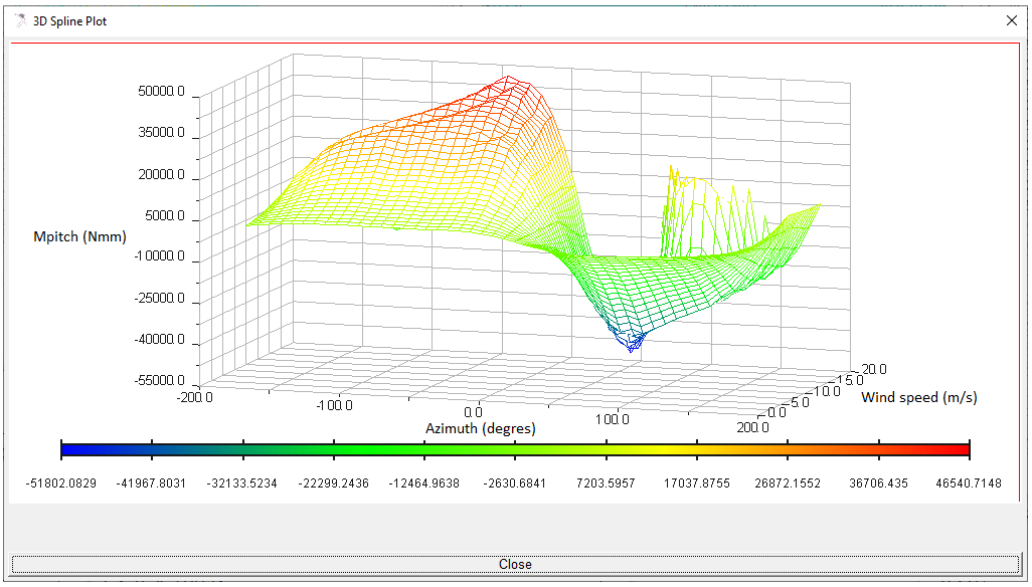

Figure 14 Load graphs (normal and tangential forces, and pitch moment) for one particular point in blade

From the collection of these predefined graphs, three load components are applied at blade's load input points attending at current X-Rotor azimuth position and wind speed. It would be possible to orient along the analysis the pitch position of upper blades, which is dependent on wind speed, but for this particular analysis, wind speed remains constant and so does the pitch.

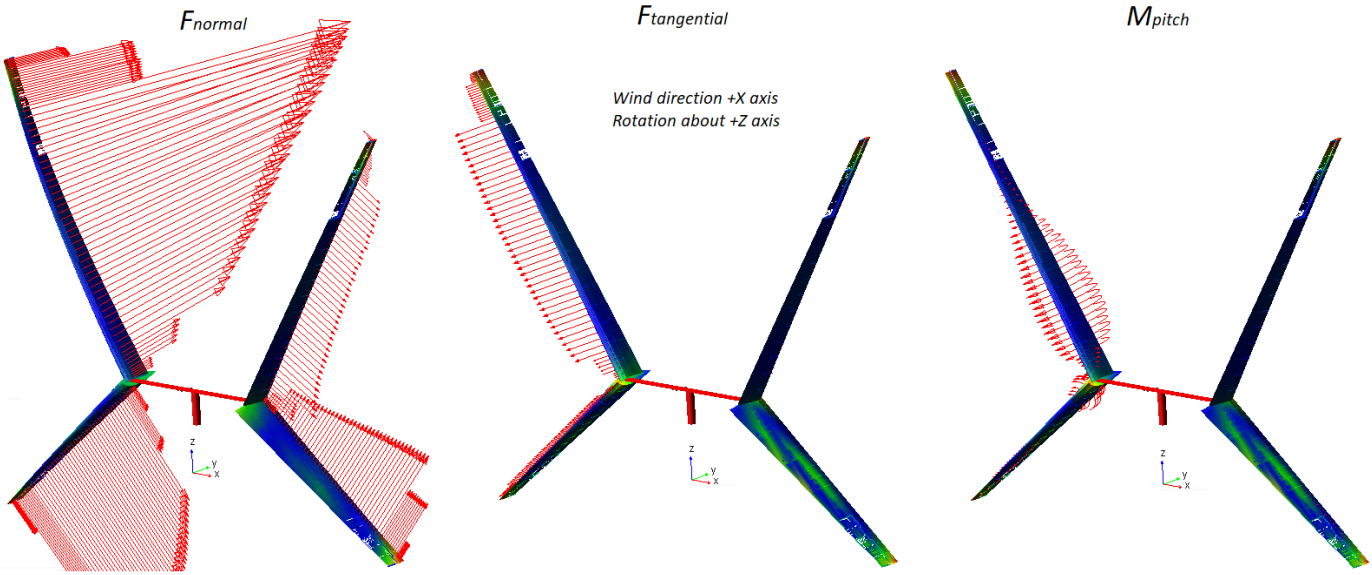

Figure 15 Direction of aerodynamic loads on blades. X-Rotor position on 90°/270° azimuth plane

Next picture shows instantaneous combined load on blades and location of load points

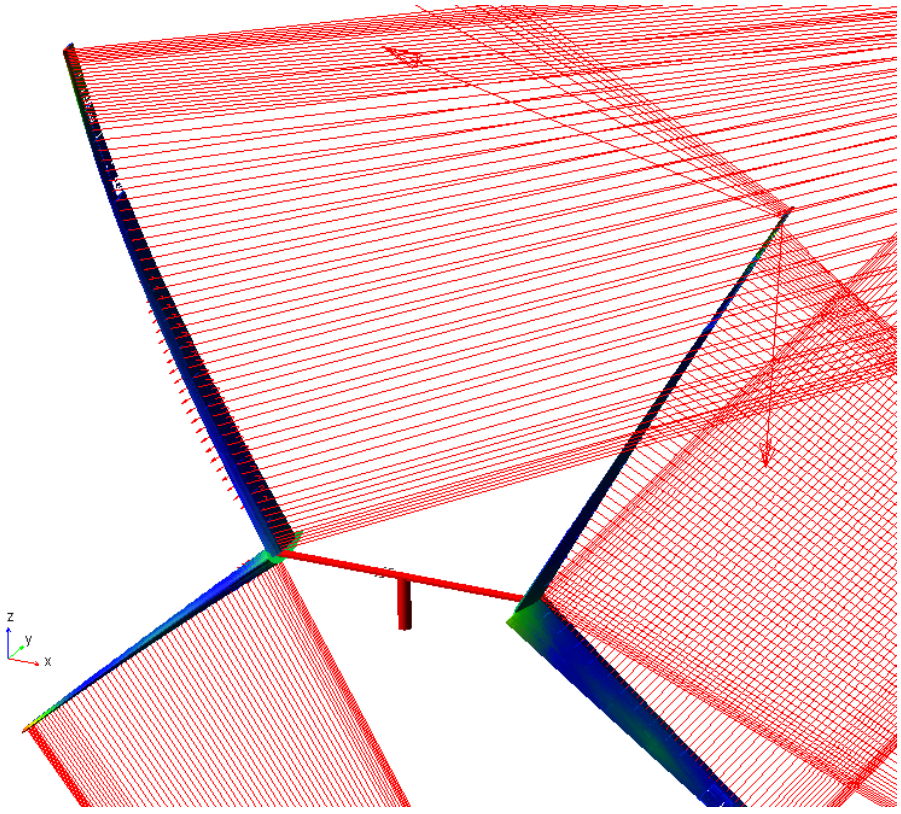

Figure 16 All points' load graphics (force and moment) at a particular time instant

Load cases description

Although model is prepared to run any constant wind speed condition, the analysis presented here correspond to one particular case, and it will be useful for showing the methodology followed to solve it.

A ***12.5m/s*** constant speed wind was considered for dynamic load case. In the stationary state, primary rotor is supposed to rotate at ***0.83rad/s*** constant angular velocity and input aerodynamic loads are defined according to rotor azimuth position. There is no control loop in the model, so to introduce the corresponding resistant torque in the system, following strategy was implemented.

Besides predefined azimuth dependent aerodynamic loads and global gravity, initial imposed rotation motion about vertical axis at constant angular velocity is declared, and after transient response decays, and a cyclic response arises, the curve of applied resistant torque by this imposed rotation along one revolution is extracted.

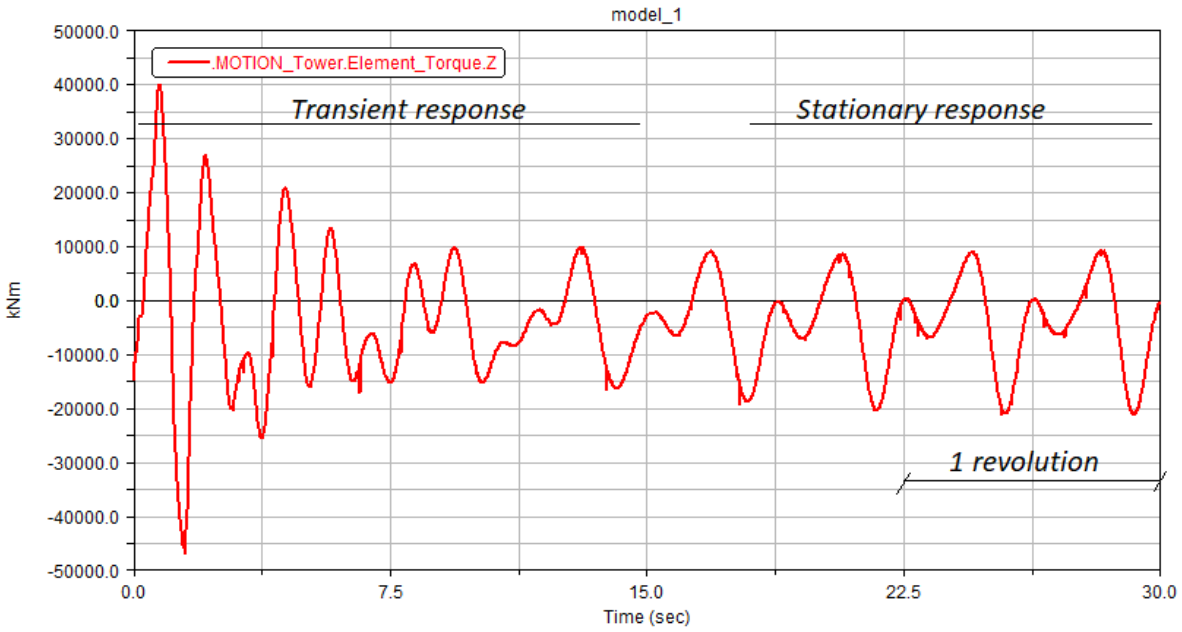

Figure 17 Torque applied (kNm) by imposed motion along 30s

The mean of this curve (integral along one revolution by time) is then considered as a constant resistant torque at tower's vertical axis for the rest of the analysis, while imposed rotation motion condition is removed. This final model, containing only loads acting on it and no forced motions, should keep its mean angular velocity along time and show minimal variation (being almost constant). Minor adjustments in the constant resistant torque assure this be the case. In the current analysis, a final 3850kNm resistant torque was applied.

cc

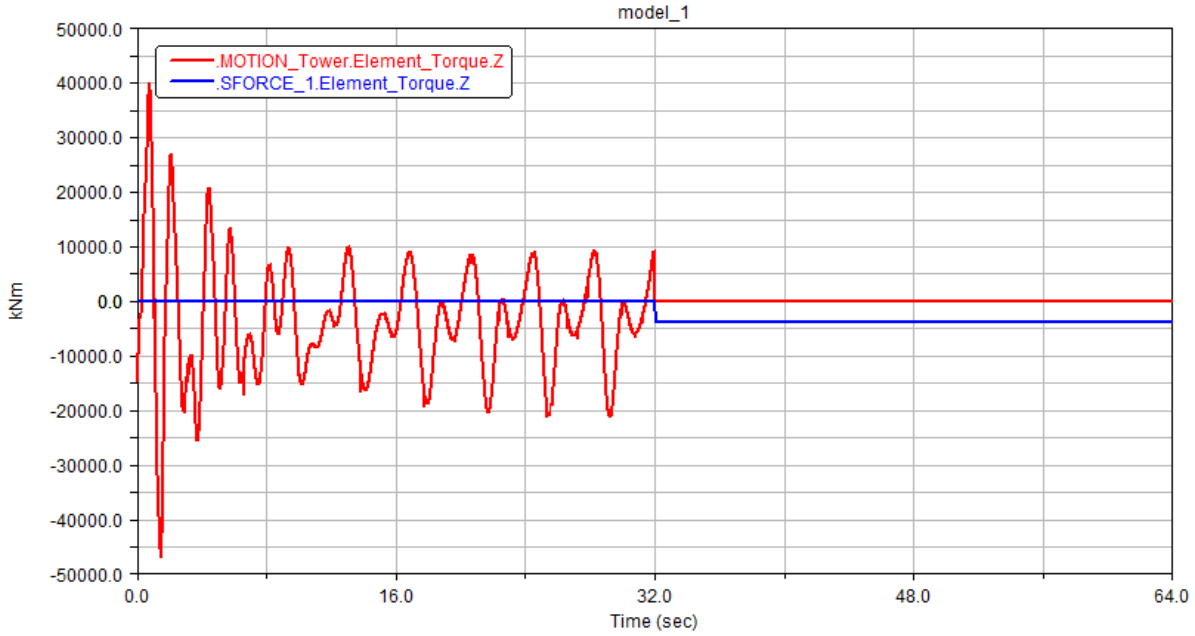

Figure 18 Torque applied (red curve, kNm) by imposed motion up to 32s, and subsequent constant applied resistant torque (blue curve, kNm) when imposed motion is turn off

Next picture superimposes the resistant torques in the model along the analysis and the angular velocity of the tower. It can be seen that after imposed motion´s turning off and constant torque application, rotation velocity remains almost constant, varying within a margin of barely a couple of degrees per second.

ccccccccccc

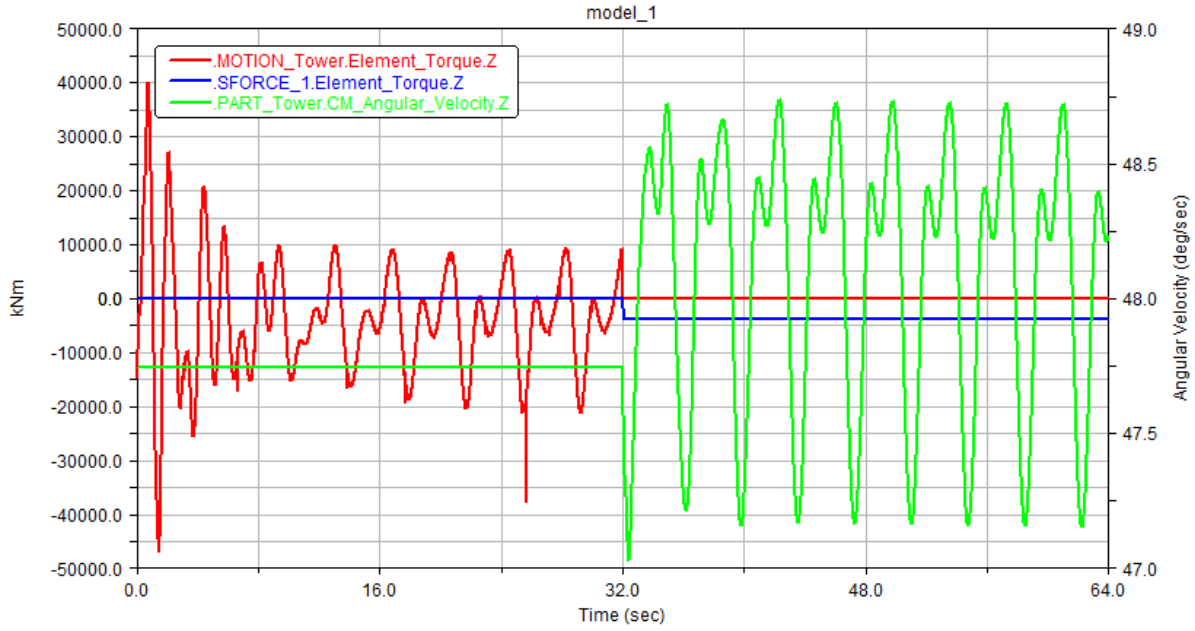

Figure 19 Torques applied (red and blue curves, kNm) along the analysis and tower angular velocity (green curve, deg/s)

Conclusions

The study focuses only on just one wind condition, but some preliminary conclusions can be extracted from the results.

Considering the constant resistant torque (3850kNm) and almost constant angular velocity (0.83rad/s), the power can easily be calculated, resulting in P = 3850x0.83 = 3210kW. This value is far below the power expected (7240kW) for this condition and wind speed.

After different design trials, as stated before, there is a number of possible misinterpretations in the model design that would increase the total power, like positioning the blade slightly ahead of the cross arm, but this should be consistent with the previous extraction of aerodynamic forces.

Another important conclusion from the results is that blades seem to be too flexible. This might question the validity of the precalculated aerodynamic loads. At this preliminary stage design, it is obvious that blade structural configuration is susceptible to change, and it would be advisable to define a stiffer configuration.

As a check, a configuration with virtual rigid blades was analyzed for the same wind conditions, and as an added result, it was found that the power increased, still under the expected values though. In the current case, the equivalent constant resistant torque goes up to 6535kNm, reaching 5446kW of power. The torque curve along one revolution in stationary state is quite different from the configuration with flexible blades.

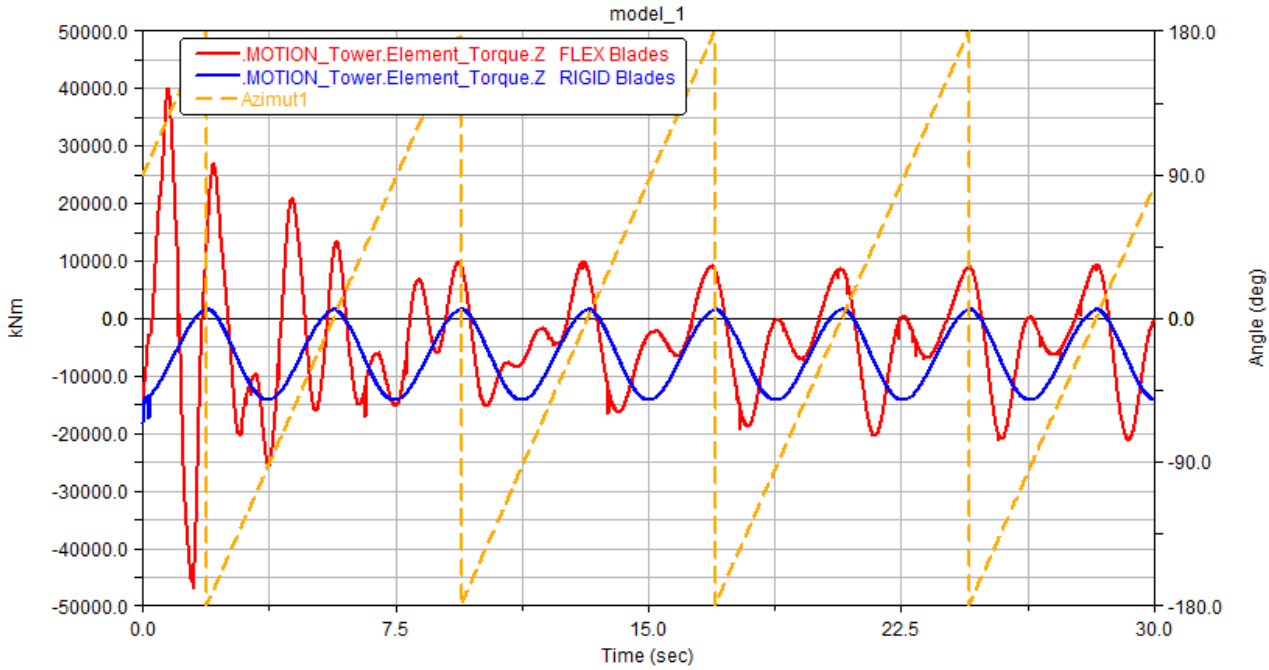

Figure 20 Torque (kNm) at tower with rigid and flexible blades, and azimuth position (deg)

A more adjusted model to real operation of X-Rotor should provide resistant torque through tangential forces at secondary rotors' positions, and being these forces azimuth dependent as well (proportional to squared relative wind speed). In any case, torque resistant summation that these both forces supply would result in the same almost constant torque as before. Additionally, the full definition of these secondary rotors would add torques at secondary generators along (normal to blade axis) and gyroscopic torques would appear, normal to both vertical primary rotor and generator axes, due to the secondary rotor inertia gyration.

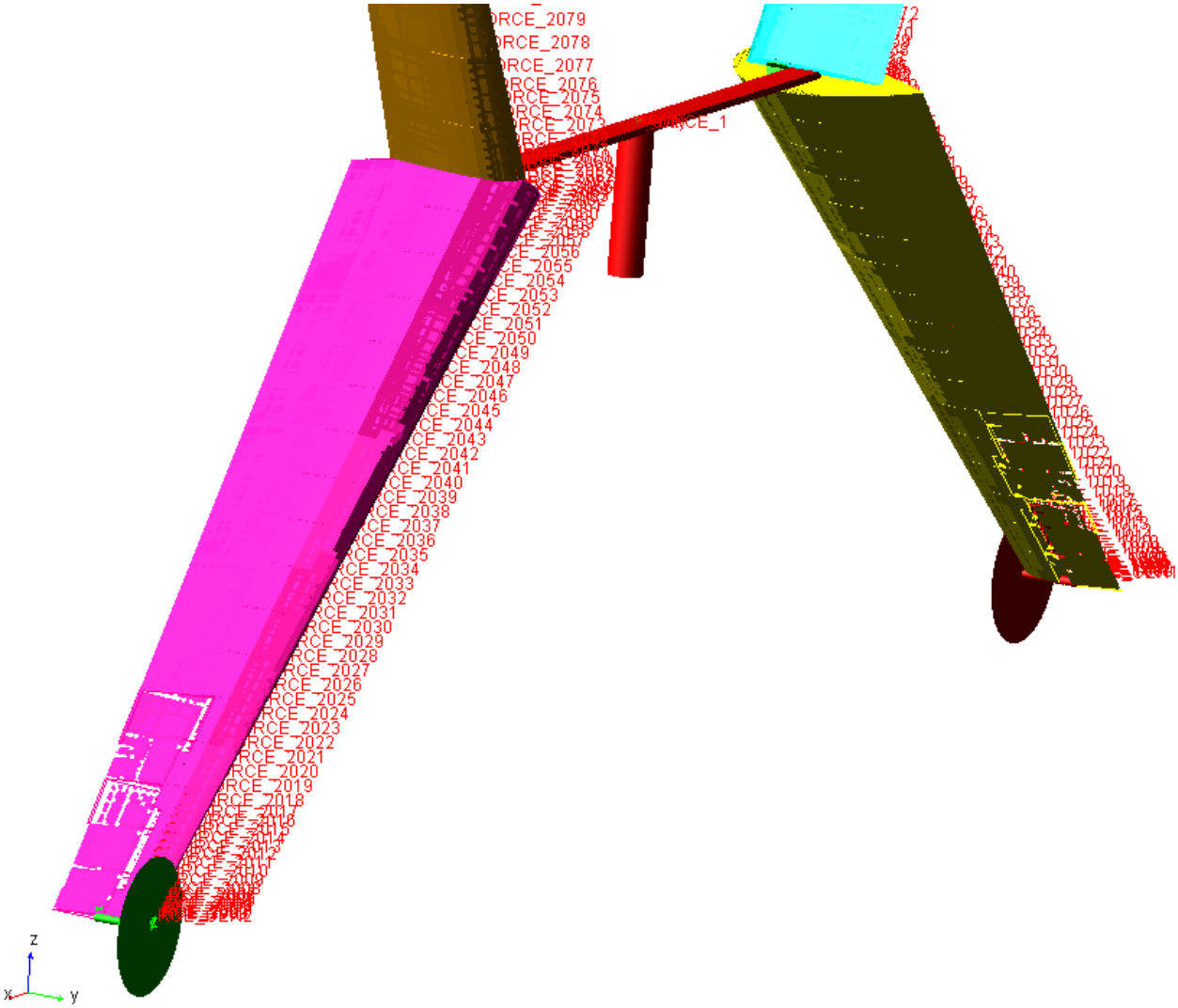

Figure 21 Structure configuration including secondary rotors at lower blades' tips

This configuration will add extra loads (thrust force and generator torque) near the lower blades' tips, worsening the problem of undesirable blade deformation (besides strength requirements). In any case, preliminary analysis simulating this configuration seems to show a lower impact of this effect than the previous one regarding deformation of lower blade, possibly due to higher blade stiffness in edge direction (thrust force direction).

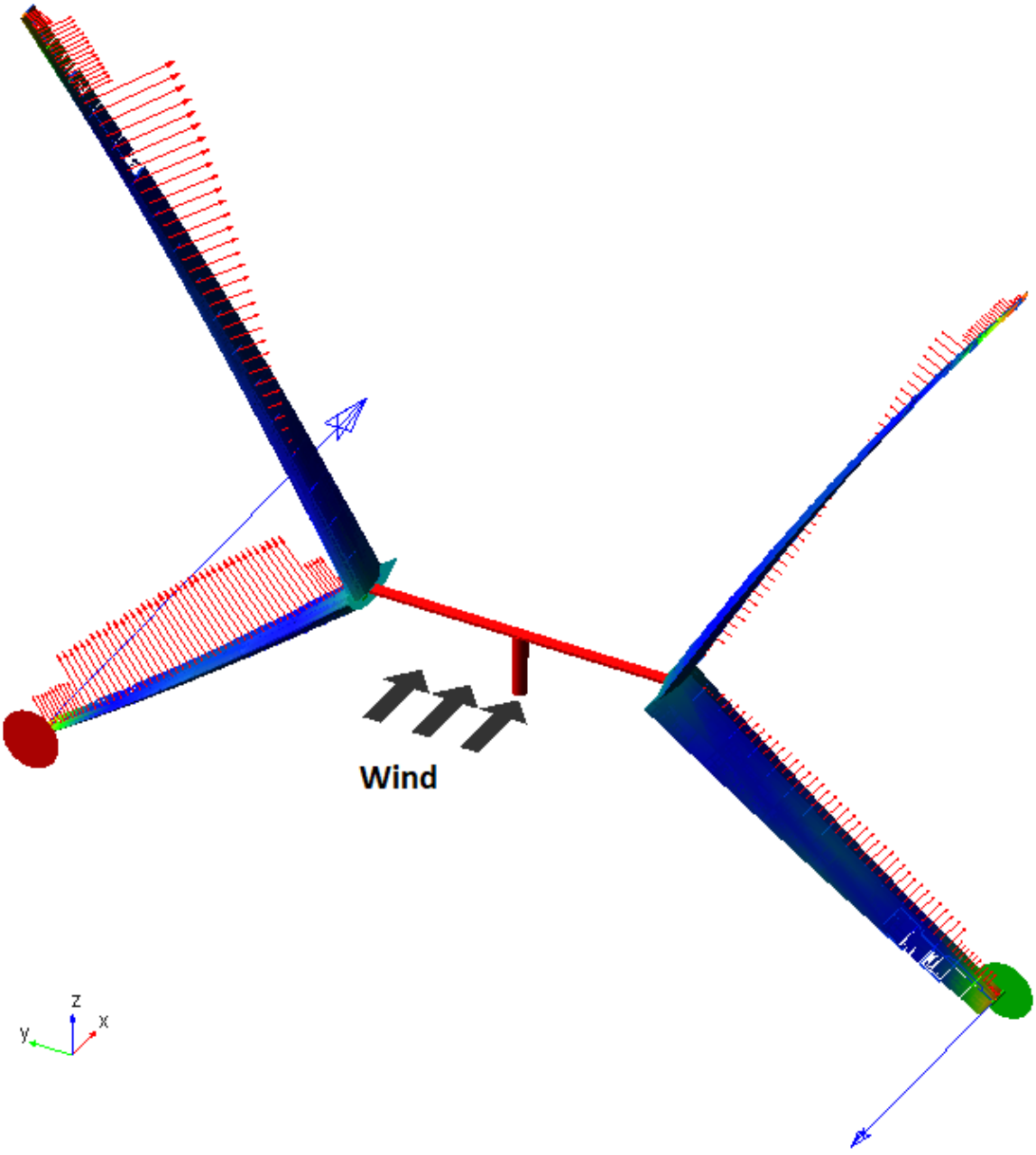

Figure 22 Load graphics with secondary rotors configuration (thrust forces in blue)

Disclaimer

Copyright Notice